第39卷第4期 无 机 化 学 学 报 Vol.39 No.4
2023年4月 CHINESE JOURNAL OF INORGANIC CHEMISTRY 765-774

利用小角度X射线散射测定八水氧氯化锆中锆结构

张智钰[1,2] 宋 静*[,3] 孙宏骞[3] 李云鹏[4] 兰 昊[2] 齐 涛[3] 田亮亮[5]
([1]中国科学技术大学稀土学院,合肥 230026)
([2]中国科学院赣江创新研究院,资源与生态环境研究所,赣州 341119)
([3]中国科学院过程工程研究所,战略金属资源绿色循环利用国家工程研究中心,北京 100190)
([4]昆明理工大学冶金与能源工程学院,昆明 650093)
([5]重庆文理学院电子信息与电气工程学院,重庆 402160)

摘要: 利用小角度X射线散射(SAXS)测量八水氧氯化锆溶液中锆的存在形式,结果表明锆在溶液中大部分是以多聚体形式存在,尤其是酸度极易对锆的聚合度产生影响。研究了八水氧氯化锆浓度、加热处理、放置时间及HCl浓度等因素对锆在溶液中存在形式的不同影响:以0.0~5.0 mol·L^{-1} HCl为溶剂,配制10~300 g·L^{-1}的氧氯化锆溶液,并考虑对溶液分别进行加热和长时间放置处理。对所配溶液进行了SAXS测试,利用Guinier方程计算了溶液中粒子的回转半径(R_g),同时利用求解最小封闭圆柱体问题的CYLview软件对溶液中锆的不同多聚体结构进行模拟计算,得到不同结构的理论R_g;通过比较R_g的实验值和计算值,确认不同条件锆液中锆粒子存在的主要形式。结果表明锆存在形式受酸度、浓度等多个因素的影响,尤其HCl的浓度是影响锆液中锆多聚体聚合度的关键;当不添加HCl时,低锆浓度溶液中锆的聚合度相对较高。

关键词: 氧氯化锆; 多聚体; 小角度X射线散射; 模拟计算
中图分类号: O614.41$^+$2 **文献标识码:** A **文章编号:** 1001-4861(2023)04-0765-10
DOI: 10.11862/CJIC.2023.041

Zr(Ⅳ) structure in aqueous zirconium chloride octahydrate solution from small-angle X-ray scattering analysis

ZHANG Zhi-Yu[1,2] SONG Jing*[,3] SUN Hong-Qian[3] LI Yun-Peng[4] LAN Hao[2] QI Tao[3] TIAN Liang-Liang[5]
([1]*School of Rare Earth, University of Science and Technology of China, Hefei* 230026, *China*)
([2]*Institute of Resources and Ecology and Environment, Ganjiang Innovation Academy, Chinese Academy of Sciences, Ganzhou, Jiangxi* 341119, *China*)
([3]*National Engineering Research Center for Green Recycling of Strategic Metal Resource, Institute of Process Engineering, Chinese Academy of Sciences, Beijing* 100190, *China*)
([4]*Faculty of Metallurgical and Energy Engineering, Kunming University of Science and Technology, Kunming* 650093, *China*)
([5]*School of Electronic Information and Electrical Engineering, Chongqing University of Arts and Sciences, Chongqing* 402160, *China*)

Abstract: In this work, the dominant structures of Zr(Ⅳ) in zirconium oxychloride octahydrate solution were measured by using small-angle X-ray scattering (SAXS). The results show that the dominant structures of Zr(Ⅳ) are in the form of polymers in the solution, and the degrees of polymerization are susceptible to acidity. The different effects of the concentration, heating treatment, standing time, and HCl concentration of zirconium oxychloride in octahydrate were studied. With 0.0-5.0 mol·L^{-1} HCl as the solvent, 10-300 g·L^{-1} zirconium oxychloride solution was prepared, moreover, the solution was heated and placed for a long time respectively. The SAXS tests were carried out for all the solutions, and the R_g experiments of the particles in the solution were calculated using the Guinier equation.

收稿日期:2022-10-08。收修改稿日期:2023-03-13。
在渝高校与中科院所属院所合作项目(No.HZ20211013)、国家重点研发计划课题(No.2019YFC1907702)和江西省双千计划(No.jxsq2020105012)资助。
*通信联系人。E-mail:jsong@ipe.ac.cn

Meanwhile, the CYLview program for solving the most minor enclosing cylinder problems was used to simulate the different polymer structures of Zr(Ⅳ) in zirconium oxychloride octahydrate solution and obtain the theoretical R_g values of different structures. By comparing the experimental R_g and the calculated R_g, the dominant structures of Zr(Ⅳ) in solution under different conditions were obtained. The results show that the dominant structures of Zr(Ⅳ) are affected by many factors such as acidity and concentration, especially the concentration of HCl is the key factor affecting the degree of polymerization. When the solvent is deionized water, the polymerization degree of zirconium is relatively high in solutions with low zirconium concentration.

Keywords: zirconium oxychloride; polymer; small-angle X-ray scattering; simulation calculation

0 Introduction

Understanding the chemistry and physicochemical properties of aqueous solutions of metal ions, which play significant roles in the fields of basic and applied chemistry, is critical. Metal ion hydrolysis[1] in aqueous solutions has received extensive attention, as it is ubiquitous. Numerous cations generally aggregate after hydrolysis and form polymeric aggregates that are linked by hydroxyl or oxygen bridges[2]. Large polymeric networks are formed, which may reach colloidal sizes, and several remain suspended in the aqueous medium as sols or precipitate in gel form[1]. The colloidal polymer significantly affects the chemistry of processes that involve heavy tetravalent cations (Th(Ⅳ), Pu(Ⅳ), and Zr(Ⅳ))[2-4]. The polymerization reactions that occur during the formation of colloidal polymers in solutions of numerous heavy tetravalent cations are affected by numerous factors, such as pH, reaction time, temperature, and concentration, and thus, these reactions are experimentally challenging. Zr(Ⅳ), as a typical heavy tetravalent cation that may form colloidal polymers in solution, is commonly the subject of numerous studies[5]. In an aqueous solution, Zr(Ⅳ) may adopt a wide variety of structures, due to its significant charge, large size, and ready ligand acceptance[6]. Zr may more often adopt a polymeric rather than monomeric form in solutions[7-8], and Zr(Ⅳ) hydrolyzes in acidic solutions to first form the tetrameric unit[9] $[Zr_4(OH)_8(H_2O)_{16}]^{8+}$ before more extensive aggregates of the tetrameric unit[7]. The hydrolysis of Zr in aqueous solutions has been previously investigated using various techniques, including Raman spectroscopy[10], wide- and small-angle X-ray scattering (SAXS)[2,9,11-12], ^{17}O nuclear magnetic resonance spectroscopy[13], extended X-ray adsorption fine structure spectroscopy[14], and ultracentrifugation[15]. The presence of $[Zr_4(OH)_8(H_2O)_{16}]^{8+}$ in highly acidic aqueous solutions has been confirmed by hydrolysis studies[2,9] and comparison with the crystal structure of $ZrOCl_2\cdot 8H_2O$ (ZOC)[15-16], which contains discrete tetrameric units. In addition, an equilibrium between the tetra- and octameric forms of $[Zr_8(OH)_{19}]^{13+}$, which affects the pH values of chloride solutions, has been suggested[17-22].

As a low-toxicity, readily available, low-cost Zr(Ⅳ) salt[23], ZOC is a widely used feedstock in preparing Zr-based catalysts. Generally, the preparation processes of catalysts and catalytic reaction processes are separate. The efficient catalysis of the transfer hydrogenation of biomass-derived molecules by the feedstock (*i.e.*, ZOC) used in catalyst preparation should be time- and energy-saving. Additionally, ZOC serves as an efficient catalyst in numerous crucial organic reactions, including the Bachmann condensation reaction, Michael additions of amines and indoles, syntheses of 1,8-dioxo-octahydroxanthene derivatives, and biomass valorization, due to its Brønsted (due to the *in situ*-formed HCl) and Lewis acidities (due to the *in situ*-generated $ZrO(OH)_2\cdot xH_2O$) in organic media[24-27]. ZOC serves as a critical raw material in producing various Zr compounds, such as stabilized ZrO_2 and mixed rare-earth oxides, as it exhibits resistance to environmental factors and various chemicals and confers superior stability[28-33]. However, clarifying the dominant species of Zr(Ⅳ) that are formed under different conditions is challenging. Therefore, this study investigated ZOC and examines Zr(Ⅳ) solutions in detail using SAXS to deter-

mine the dominant species in Zr(Ⅳ) solutions under different experimental conditions. Meanwhile, the corresponding structures of the dominant species were calculated and designed using the simple program CYLview[34].

1 Experimental

The aqueous Zr(Ⅳ) stock solutions were prepared by dissolving ZOC crystalline material (supplied by Jiangxi Jing′an High Tech, Nanchang, China) in deionized water or different concentrations of HCl to explore the effects of four factors on the dominant species within the solutions, *i.e.* ρ_{ZOC}: 10, 50, or 300 g·L^{-1}; Heating treatment: 298 or 353 K; Standing time: 1, 30, or 60 d; c_{HCl}: 0.5, 1, 2, 4, or 5 mol·L^{-1}.

These samples were analyzed using the Guinier law of SAXS and the structures of the dominant species within the Zr (Ⅳ) solutions were modeled using the program CYLview. Small - angle scattering is widely applied in determining particle sizes and, in several cases, their geometries, and thus, SAXS was adopted in this study. Based on the SAXS measurements, determining the electronic radii of gyration (R_g) of particles and the absolute intensity at zero angles, which was not established in previous experimental studies, is possible[25]. With these two physical quantities, novel structural data regarding the polymeric Zr species in the solutions could be obtained. CYLview enables a rigorous, automatic method of determining the parameters of a cylinder by continuously adjusting them so that the cylinder encloses all atoms, minimizing the size of the cylinder.

SAXS was conducted at Anton Paar using a Cu $K\alpha$ radiation source, and scattering patterns were collected using an Eiger R 1M Horizontal detector with a resolution of 1030×1065 pixels. The image exposure time and X-ray wavelength were 3×300 s and 0.154 2 nm, respectively, and the distance between the detector and sample was 197.034 mm. The sample scattering was corrected for detector sensitivity, dark current, and the background solvent. The background scattering using an HCl solution (or deionized water) was measured in the same cell with the same concentration of HCl as that in the sample. Moreover, the results of SAXS were identical, regardless of whether HCl solution or deionized water was used, and thus, when we analyzed the results, the background scattering was ignored. The Origin program was used to produce intensity contour plots and perform standard analyses (*e.g.*, Guinier plots).

2 Simulation theory

X-ray scattering depends on the number of particles, the electron contrast between the particle and medium, and the sizes of the particles[35]:

$$I(q)=I_g(q)N_P(\Delta\rho V)^2\exp(-q^2R_g^2/3) \quad (\mathbf{1})$$

where V is the volume of the particle, N_P is the number of particles per unit volume, R_g is the radius of gyration, I_g is the scattering intensity due to a single electron, $\Delta\rho$ is the electron density difference between the particle and medium, and q is the scattered wave vector, $q=4\pi\sin\theta/\lambda$, where 2θ is the scattering angle and λ is the X-ray wavelength.

Based on Eq.**1**, the plot of ln I vs q^2 should be linear and the R_g of the particle may be determined using the slope of this line. The Guinier law is at least valid for $q\leqslant 1/R_g$, and it is not a function of the particle shape in this range of q. The Guinier law is shown in Eq.**2**:

$$\ln I=I(0)\exp(-q^2R_g^2/3) \quad (\mathbf{2})$$

The intensity at zero angles, $I(0)$, which is obtained by the extrapolation of the Guinier law to q=0, yields data regarding the numbers of particles and electrons in each particle:

$$I(0)=I_g(q)N_P(\Delta\rho V)^2 \quad (\mathbf{3})$$

Eq.**1** and **3** are originally developed for monodisperse particles. In polydisperse systems, $I(0)$ and the observed R_g may be expressed as follows[35]:

$$R_g^2=\sum_{i=1}^{n}[N_{P,i}(\Delta\rho_i V_i)^2R_{g,i}^2]/\sum_{i=1}^{n}N_{P,i}(\Delta\rho_i V_i)^2 \quad (\mathbf{4})$$

$$I(0)=I_g(0)N_{P,i}(\Delta\rho_i V_i)^2 \quad (\mathbf{5})$$

Where $N_{P,i}$ is the number density of the ith particle, V_i is the volume of the particle, $R_{g,i}$ is the radius of gyration of the ith particle, and $\Delta\rho_i$ is the difference in the electron densities of the particle and medium.

The Guinier law does not yield data regarding the shape of the particle, and thus, this should be deter-

mined via the calculation of a complete scattering curve. There are three potential geometries within the ZOC solution: a sphere, a cylinder, and an ellipsoid of revolution[2]. Overall, the three geometries exhibit few differences, as the aspect ratio is relatively small, and the cylinder is more closely related to the shape of the particle[17]. Therefore, the structures were modeled with the assumption that the particle shapes were cylindrical. The R_g values of all common shapes may be calculated using the formulas shown in Table 1 after the parameters are obtained using CYLview.

Table 1 Formulas used to calculate the R_g values of various common shapes

Shape	Formula
Ball (radius: r)	$(3/5)^{0.5}r$
Spherical shell (outer radius: r, inner radius: r_{in})	$(3/5)^{0.5}\{[1-(r_{in}/r)^5]/[1-(r_{in}/r)^3]\}^{0.5}r$
Ellipsoid (radius: r, r, r_v)	$\{[2+(r_v/r)^2]/5\}^{0.5}r$
Cylinder (length: $2l$, diameter: $2r$)	$[(r^2/2)+(l^2/3)]^{0.5}$
Thin disk (radius: r)	$2^{0.5}r$
Fine fiber (length: $2l$)	$3^{0.5}l$
Parallelepiped (side length: $2a$, $2b$, $2c$)	$[(a^2+b^2+c^2)/3]^{0.5}$
Cube (side length: $2a$)	a

3 Results and discussion

The Guinier plots of ln I as a function of q^2 of all samples yielded the R_g values. The Guinier plots of the HCl solutions (or deionized water) were virtually straight lines, which were not included in the analysis. Furthermore, the R_g values of the models were obtained using CYLview.

3.1 Effect of mass concentration of ZOC

The typical plots of ZOC solutions with concentrations of 10, 50, and 300 g·L^{-1} in deionized water are shown in Fig.1. Clearly, at ρ_{ZOC}=10 and 50 g·L^{-1}, linear plots were obtained (except at extremely low I, where the beam stop interferes with proper intensity determination). The linearity of the plot further indicates the monodispersity of the Zr(Ⅳ) system. The R_g values were not very different, and thus, the dominant species did not change with ρ_{ZOC}. However, a nonlinear region was observed at 300 g·L^{-1} of ρ_{ZOC}, which may be due to the contribution of interparticle interference. The linear regions exhibited slopes that yield R_g values of 0.550 nm. Despite the wide variance in concentration, the constant R_g indicates that the cause of the nonlinear region does not significantly influence the linear region of the Guinier plot. Therefore, the most direct approach considers the linear region as indicative of the behaviors of the independent particles.

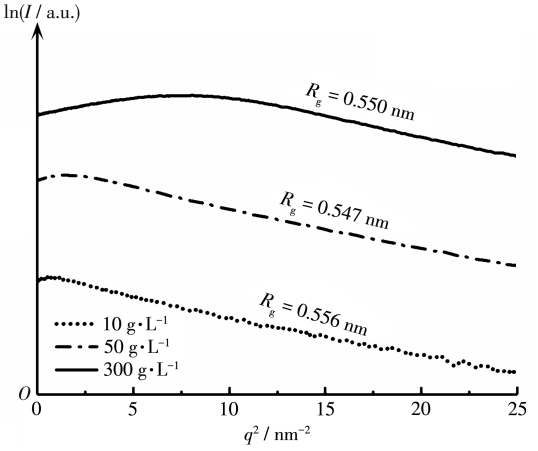

Fig.1 Guinier plots for different ZOC concentrations in one day

In addition, at very low q^2 values, the observed small dome shape was due to the mutual repulsion between particles in the solution, which is generally caused by electrostatic interactions. As the Cl^- in ZOC is free, the repulsion effects of the particles at 300 g·L^{-1} of ρ_{ZOC} are clearer, whereas, at the medium and low concentrations (10 and 50 g·L^{-1}), the interparticle repulsion effects only manifest at low q^2 values. However, the dominant species are consistent in the aqueous ZOC solutions with different concentrations.

3.2 Effect of heating treatment

As shown in Fig.2, the R_g values and shapes of the Guinier plots differed considerably at ρ_{ZOC} of 10 and 50

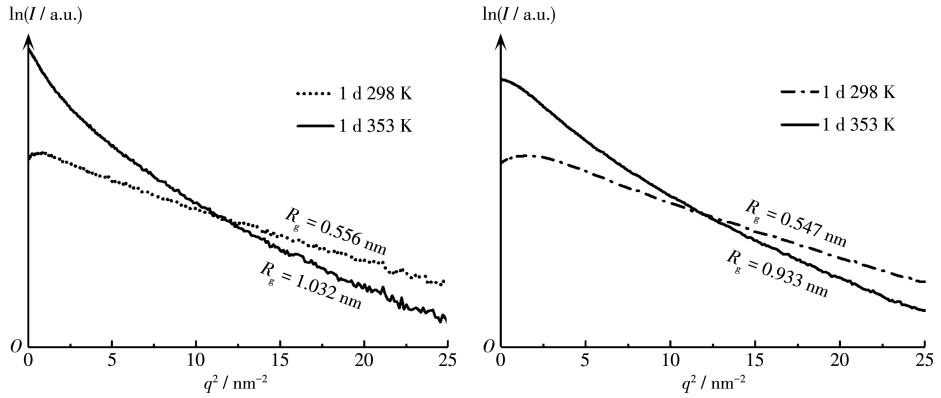

Fig.2　Guinier plots for heating treatment (Left: 10 g·L^{-1}; Right: 50 g·L^{-1})

g·L^{-1} after heating. The upper dome shape is due to the repulsion between the particles, whereas after heating, concave shapes were observed, and thus, heating may cause particle aggregation. The particles gain additional energy due to the heating, which is partially used to counteract the repulsive forces between the particles, and the remaining energy should also induce particle aggregation. As a result, the quality of the dominant particles in the solution should increase considerably, accelerating particle aggregation in the solution. Due to the distinction between the results obtained at ρ_{ZOC}= 300 and 10 or 50 g·L^{-1}, the Guinier plot obtained at 300 g·L^{-1}, which is shown in Fig.3, is analyzed separately.

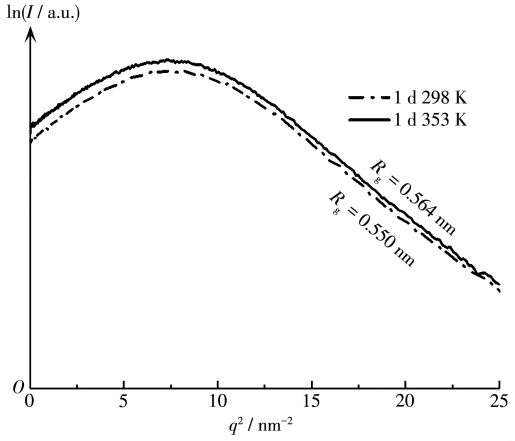

Fig.3　Guinier plots for heating treatment at 300 g·L^{-1} of ρ_{ZOC}

The Guinier plots at 298 and 353 K displayed virtually no changes at ρ_{ZOC}=300 g·L^{-1} after heating. As shown in Fig. 3, the upper dome shape was still observed, *i. e.*, the repulsion between particles is so high that the extra energy provided to the particles via heating may not overcome the repulsion at the high concentration. Numerous particles occur in a unit volume at ρ_{ZOC}=300 g·L^{-1}, and thus, the repulsion between particles is further increased. Compared with those at medium and low concentrations, the types of particles present in the high - concentration solution are more complex (the nonlinear region in the Guinier plot was larger), and thus, the energy provided via heating is insufficient to overcome the interparticle repulsion and cause particle aggregation. Thus, the shape of the plot at 353 K was the same as that at 298 K.

3.3　Effect of standing time

According to the concentration of ZOC, the analysis of standing time should also be divided into two cases (Fig.4 and 5). As shown in Fig.4, the R_g values increased slightly with the standing time, which is mainly due to an increase in the free Cl^- in the solution. As the standing time increases, the Cl^- within the solution should be incorporated into the particle structure and the overall charge should decrease, and the charges of several particles should even change from positive to neutral. Neutral particles are also more stable in solution.

In the Guinier plot at the high concentration, the standing time exhibited virtually no effect on the R_g values, as shown in Fig. 5. The plots at 30 and 60 d appeared to be parallel, and thus, the tolerance of the species toward Cl^- has reached a saturated state at 300 g·L^{-1}. Generally, the standing time displays little effect on the general structures of the dominant species in ZOC solutions, and the effect is mainly reflected in

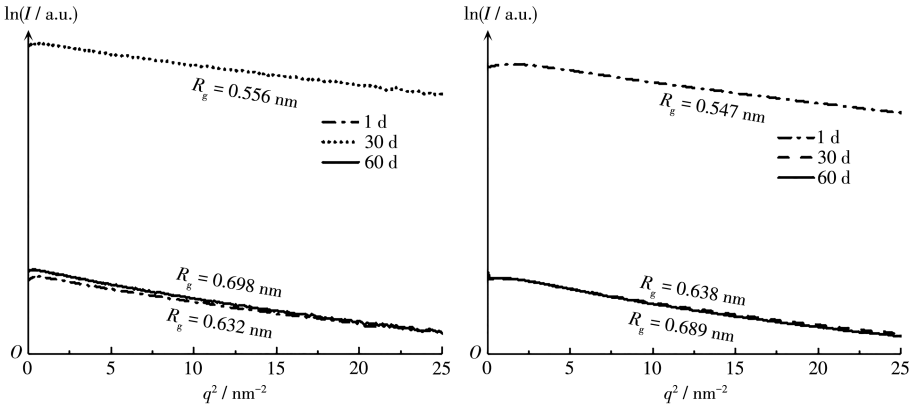

Fig.4 Guinier plots for standing time at 10 g·L^{-1} (left) and 50 g·L^{-1} (right) of ρ_{ZOC}

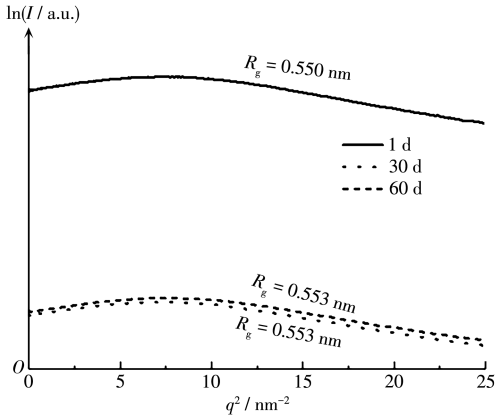

Fig.5 Guinier plots for standing time at ρ_{ZOC}=300 g·L^{-1}

terms of the free Cl^- at medium and low concentrations.

3.4 Effect of concentration of HCl

The influences of the HCl concentration were analyzed in three cases: 10, 50, and 300 g·L^{-1} of ZOC, and all samples were allowed to stand for 30 d. Notably, when ρ_{ZOC}=300 g·L^{-1} and c_{HCl}=5 mol·L^{-1}, crystals were formed, and thus, this case is not analyzed here.

As shown in Fig. 6, the Guinier plots of all samples were linear, and thus, the dominant species in the solutions were homogeneous at 10 g·L^{-1}. Remarkably, a horizontal line was observed at c_{HCl}>2 mol·L^{-1}, potentially because Zr^{4+} is the dominant species under these conditions. This experimental phenomenon is consistent with the conclusions of Clearfield[7] and Devia[8], who reported the existence of the monomeric species Zr^{4+} under specific conditions, with a low ρ_{ZOC} and high c_{HCl} value. Remarkably, the R_g values in deionized water and c_{HCl}=0.5 mol·L^{-1} were 0.632 and 0.250 nm, respectively, and the former was much larger than the latter. Therefore, Cl^- inhibits the formation of multimers of the dominant species. No Zr—Cl bonds are present in ZOC crystals, and thus, the electrostatic forces generated by Cl^- are larger than the binding forces between the Zr polymers.

As shown in Fig. 7, R_g decreased regularly with increasing c_{HCl} at ρ_{ZOC}=50 g·L^{-1}. Overall, the degree of polymerization of the dominant species in the solution

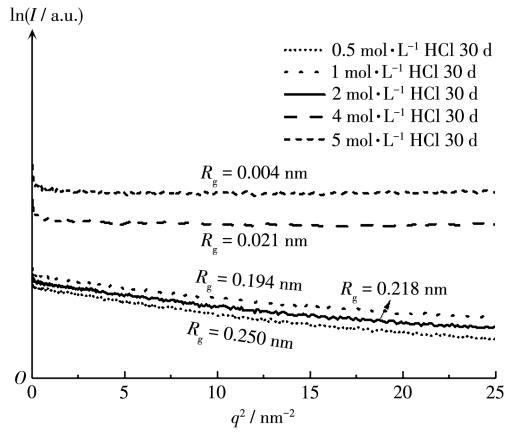

Fig.6 Guinier plots for c_{HCl} at ρ_{ZOC}=10 g·L^{-1}

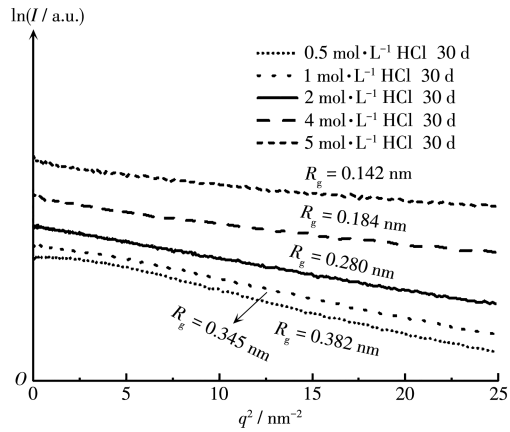

Fig.7 Guinier plots for c_{HCl} at ρ_{ZOC}=50 g·L^{-1}

decreased with increasing c_{HCl}. The concentration of Zr increases, and thus, even at a high c_{HCl}, the dominant species is still present in aggregates rather than in the ionic state. Therefore, the Zr salt is essentially a polymer in solution.

The situation is even more complex at ρ_{ZOC}=300 g·L^{-1}, as shown in Fig.8. As c_{HCl} was varied from 0 to 4 mol·L^{-1}, the Guinier plot changed from arched to linear, *i. e.*, the linear region of the Guinier plot increased with increasing c_{HCl}, which indicates that increasing c_{HCl} promotes homogenization of the species in the ZOC solution. However, R_g still decreased with increasing c_{HCl}, which is mainly due to the inhibition of the polymerization of the Zr-containing species by Cl$^-$.

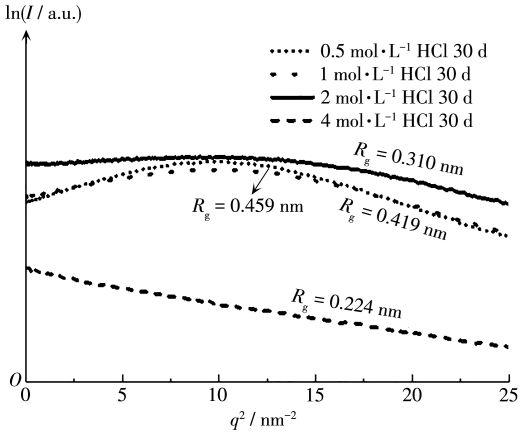

Fig.8　Guinier plots for c_{HCl} at ρ_{ZOC}=300 g·L^{-1}

In summary, among the four influencing factors, the ρ_{ZOC} and c_{HCl} exhibit the highest influences on the dominant species in the ZOC solution. Furthermore, the R_g values of all experimental samples were obtained using the Guinier plots. However, the structures of the dominant species in the solutions were not analyzed, and thus, they were simulated and calculated.

3.5　Modeling the structures of the dominant Zr(Ⅳ) species

The R_g values indicating the dominant Zr(Ⅳ) species under different experimental conditions were obtained via the Guinier analyses of the results of SAXS. Under the conditions of low ρ_{ZOC} and high c_{HCl}, the ions are the dominant species in the solution, according to the results of the experimental analyses and the corresponding literature. Under other conditions, the dominant species occur as polymers, but the types of polymers in the solutions are unclear. Therefore, several possible structures, which are based on the crystal structure data of the ZOC single crystal[7], were constructed, as shown in Fig.9. In these models, the H atoms may be ignored, as they are always combined with O atoms. The O atoms shown in Fig.9 represent two formations: OH (double hydroxyl bridging bonds, 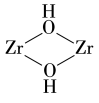) and H_2O. The construction of the

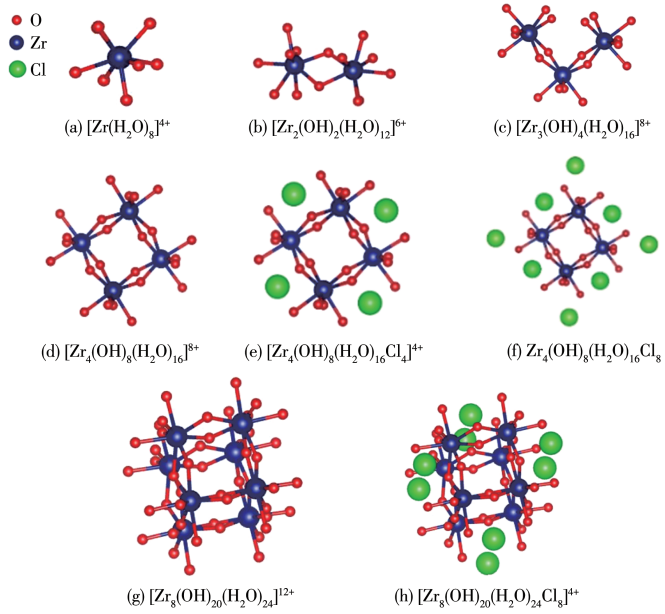

Fig.9　Possible chemical structures of the dominant species fo ZOC

octamer was based on the related research of Singhal[17], but unfortunately, the details of the octamer species were not previously analyzed. Therefore, the number of chlorides in the octamer was calculated based on the octamer data. The octamer is formed by two stacked tetramers, $[Zr_4(OH)_8(H_2O)_{16}]^{8+}$, which are connected by —OH—, and Cl^- is pivotal in the formation of the dominant species within the ZOC solutions, particularly at a high c_{HCl}.

As a Cl^- occurs around each bond that connects two tetramers due to electrostatic neutralization, the octamers contain up to 20 chloride ions in their structures. The Cl^- close to the H_2O (denoted Cl1) attached to the Zr atom is further analyzed. Compared to the Cl^- close to the double oxygen bridge (denoted Cl2), Cl1 is more likely to be free in the water, *i.e.*, the Cl1 site is likely not part of an octamer or a tetramer in the solution, which is partly due to the high dielectric constant of the solute. Therefore, the number of Cl^- in the octameric form ranges from 0 to 12, and thus, all possible structures are designed.

3.6 Calculation of the R_g values of the structures and analysis of the dominant species in the solutions

The raw data were obtained from the coordinates of each atom in the crystal structure, and the Supporting information contains more details regarding the atomic coordinates of each structure. The parameters of the simulated structures were then calculated in CYLview, using the conversion formula of the cylinder shown in Table 1 to yield the R_g of each simulated structure. To match the experimental value to the simulated value more closely, several structures with additional chloride ions were calculated via interpolation based on the original structure. Table 2 shows the calculated R_g of each chemical structure. There are only three boundary conditions, according to a theoretical analysis, in terms of the number of Cl^- in an octamer: 0, 8, and 12. Therefore, based on the boundary conditions, an increase in Cl^- was considered to obtain more accurate structures of the octamer, as shown in Table 2.

As shown in Table 2, the calculated R_g values were in a range of 0.166-0.664 nm, whereas the measured R_g values were between 0.004 and 1.032 nm. To realize the accuracies of the designed structures, we adopted a novel method: the effective sampling rate. It may be defined as the number of samples within the calculated range as a percentage of the total number of samples measured. However, several samples may be excluded from the total number of samples measured: R_g=0.004, 0.021, 0.933, 1.032 nm. The forms of the ions at a high c_{HCl} and low ρ_{ZOC} yield measured R_g values under these conditions of approximately 0 nm, which are consistent with values of 0.004 and 0.021 nm. The effective sampling rate obtained by excluding those samples was 95%. The other measured values were all perfectly consistent with the constructed chemical models within the error range.

Table 2 Calculated R_g of each chemical structure

Code of structure	Chemical structure of species model	R_g / nm
a	$[Zr(H_2O)_8]^{4+}$	0.166
b	$[Zr_2(OH)_2(H_2O)_{12}]^{6+}$	0.278
c	$[Zr_3(OH)_4(H_2O)_{16}]^{8+}$	0.321
c	$[Zr_3(OH)_4(H_2O)_{16}Cl_2]^{6+}$	0.367
d	$[Zr_4(OH)_8(H_2O)_{16}]^{8+}$	0.371
e	$[Zr_4(OH)_8(H_2O)_{16}Cl_4]^{4+}$	0.414
f	$Zr_4(OH)_8(H_2O)_{16}Cl_8$	0.459
g	$[Zr_8(OH)_{20}(H_2O)_{24}]^{12+}$	0.510
g	$[Zr_8(OH)_{20}(H_2O)_{24}Cl_4]^{8+}$	0.556
g	$[Zr_8(OH)_{20}(H_2O)_{24}Cl_6]^{6+}$	0.609
h	$[Zr_8(OH)_{20}(H_2O)_{24}Cl_8]^{4+}$	0.640
h	$Zr_8(OH)_{20}(H_2O)_{24}Cl_{12}$	0.664

Here, several explanations for the larger values are provided. Firstly, the experimental conditions should be noted: fresh, heating, 10 and 50 $g\cdot L^{-1}$. Remarkably, under these conditions without heating, the measured R_g values are 0.556 and 0.547 nm, which are consistent with the structure of the octamer with a certain amount of Cl^-. However, other particles occur in the solution, and the solution of dissolved ZOC crystals in deionized water is acidic. Additionally, at a lower acidity, the dominant form in the ZOC solution is the octamer. Therefore, numerous octamers occur in the solution under these conditions without heating, and heating may cause partial aggregation. Thus, polymerization is very likely to occur when large amounts of the two species occur in a solution.

A few changes in the R_g values at ρ_{ZOC}=10 and 50 $g\cdot L^{-1}$ are observed after standing for a few days. These changes are mainly because the number of chloride ions in the dominant species also changes slightly with increasing standing time, and the change may be expressed by the following chemical formula (ρ_{ZOC}=10 or 50 $g\cdot L^{-1}$):

30 d: $[Zr_8(OH)_{20}(H_2O)_{24}Cl_4]^{8+}+4Cl^- \rightarrow [Zr_8(OH)_{20}(H_2O)_{24}Cl_8]^{4+}$ (**6**)

60 d: $[Zr_8(OH)_{20}(H_2O)_{24}Cl_8]^{4+}+4Cl^- \rightarrow Zr_8(OH)_{20}(H_2O)_{24}Cl_{12}$ (**7**)

Additionally, the effect of HCl at different mass concentrations of ZOC may be explained by the chemical equations shown in Fig.10. As the concentration of HCl increases, at almost all ρ_{ZOC} values, the degree of polymerization of the dominant species in the solution decreases. Only at very high c_{HCl} and very low ρ_{ZOC} should the Zr in solution occur in an ionic state, whereas under other conditions, it should appear as a polymer.

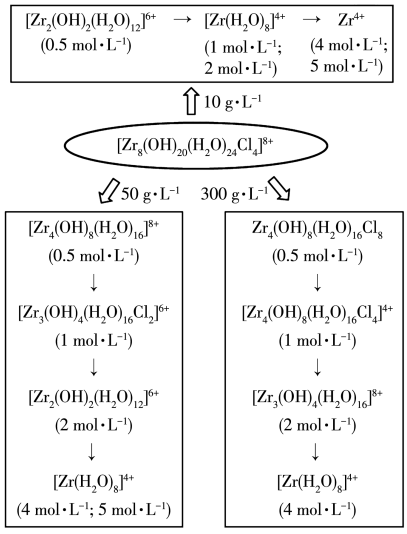

Fig.10　Chemical equations representing the effect of HCl

4　Conclusions

SAXS has been used to determine the sizes and geometries of small polymeric structures in $ZrOCl_2\cdot 8H_2O$ (ZOC) solutions under different conditions, which was impossible using other experimental techniques. In this study, Guinier analysis was used to calculate the R_g values under various experimental conditions, and the chemical structures of various species were modeled according to the crystal structure of ZOC. The spatial coordinates of each atom corresponding to the chemical structure were then obtained, and the CYLview program was used to calculate and convert the R_g of each simulated structure. Upon comparing the measured R_g with the simulated R_g to determine the structure of the main species occurring under each condition, the degree of matching was approximately 95%. We also identified two extreme cases via experimental measurements and analyzed the causes of these phenomena: the smaller R_g values are due to the ionic forms in the ZOC solutions, and the larger R_g values are due to the polymerization of tetra- and octamers. This study covers the dominant species within ZOC solutions under various conditions, which are of considerable significance in theoretical research in the Zr industry.

Acknowledgments: We acknowledge financial support from the cooperative project between universities in Chongqing and institutes affiliated with the Chinese Academy of Sciences (Grant No.HZ2021013), the sub-project of the National Program on Key Research Project (Grant No. 2019YFC1907702), and the Double Thousand Plan of Jiangxi Province (Grant No. jxsq2020105012).

Supporting information is available at http://www.wjhxxb.cn

References:

[1]Gandini A, Belgacem M N. Furans in polymer chemistry. *Prog. Mater.*

Sci., **1997**,**22**(6):1203-1379

[2]Toth L M, Lin J S, Felker L K. Small-angle X-ray scattering from zirconium(Ⅳ) hydrous tetramers. *J. Chem. Phys.*, **1991**,**95**:3106-3108

[3]Nyman M. Small-angle X-ray scattering to determine solutions speciation of metal-oxo clusters. *Coord. Chem. Rev.*, **2017**,**352**:45-48

[4]Wang Z, Xin X, Zhang M, Li Z, Lv H J, Yang G Y. Recent advances of mixed-transition-metal-substituted polyoxometalates. *Sci. China-Chem.*, **2022**,**65**:1515-1525

[5]Li M, Zhao Z, Yin P C. Small-angle X-ray scattering studies of emergent polyoxometalates in solution. *J. Coord. Chem.*, **2020**, **73**(17/18/19):2365-2372

[6]Ziebarth R P, Corbett J D. Centered zirconium chloride clusters. Synthetic and structural aspects of a broad solid-state chemistry. *Acc. Chem. Res.*, **1989**,**22**(7):256-262

[7]Stojilovic N, Bender E T, Ramsier R D. Surface chemistry of zirconium. *Prog. Surf. Sci.*, **2005**,**78**(3/4):101-184

[8]Devia D H, Sykes A G. Aqueous solution chemistry of zirconium(Ⅳ). 1. Kinetic studies on hydrogen ion and general acid (HX) induced dissociations of the tetrameric ion $(Zr_4(OH)_8(H_2O)_{16})^{8+}$. *Inorg. Chem.*, **1981**, **20**(3):910-913

[9]Tera H, Aberg C. Strength of knots in surgery in relation to type of knot, type of suture material and dimension of suture thread. *Acta Chirurgica Scandinavica*, **1977**,**143**(2):75-83

[10]Hannane S B F, Bouix J. Raman spectrometric and proton NMR study of Zr(Ⅳ) hydrolysis in aqueous solution. Ⅱ. Quantitative study. *Bull. Soc. Chim. Fr.*, **1990**,**127**(1/2/3/4):50-56

[11]Jutson J A, Richardson R M, Jones S L. Norman C. Small angle X-ray scattering studies of polymeric zirconium species in aqueous solution //Higgins S. *Materials research society symposia proceedings*: *Vol*.180. Cambridge: Cambridge University Press, **1990**:123-127

[12]Muha G M, Vaughan P A. Structure of the complex ion in aqueous solutions of zirconyl and hafnyl oxyhalides. *J. Chem. Phys*., **1960**,**33**: 194-199

[13]Åberg M, Glaser J. ^{17}O and ^{1}H NMR study of the tetranuclear hydroxo zirconium complex in aqueous solution. *Inorg. Chim. Acta*, **1993**,**206**:53-61

[14]Dewald H D. Use of EXAFS to probe electrode-solution interfaces. *Electroanalysis*, **1991**,**3**(3):145-155

[15]Johnson J S, Kraus K A. Hydrolytic behavior of metal ions. Ⅵ. Ultracentrifugation of zirconium(Ⅳ) and hafnium(Ⅳ); Effect of acidity on the degree of polymerization. *J. Am. Chem. Soc.*, **1956**,**78**(16):3937-3943

[16]Mak T C W. Refinement of the crystal structure of zirconyl chloride octahydrate. *Can. J. Chem.*, **1968**,**46**:3491-3497

[17]Singhal A, Toth L M, Lin J S, Affholter K. Zirconium(Ⅳ) tetramer/octamer hydrolysis equilibrium in aqueous hydrochloric acid solution. *J. Am. Chem. Soc.*, **1996**,**118**:11529-11534

[18]Walther C, Rothe J, Fuss M, Büchner S, Koltsov S, Bergmann T. Investigation of polynuclear Zr(Ⅳ) hydroxide complexes by nanoelectrospray mass-spectrometry combined with XAFS. *Anal. Bioanal. Chem.*, **2007**,**388**:409-431

[19]Gossard A, Toquer G, Grandjean S, Grandjean A. Coupling between SAXS and Raman spectroscopy applied to the gelation of colloidal zirconium oxy-hydroxide systems. *J. Sol-Gel Sci. Technol.*, **2014**,**71**: 571-579

[20]Kobayashi T, Nakajima S, Motokawa R, Matsumura D, Saito T, Sasaki T. Structural approach to understanding the solubility of metal hydroxides. *Langmuir*, **2019**,**35**:7995-8006

[21]Bremholm M, Birkedal H, Iversen B B, Pedersen J S. Structural evolution of aqueous zirconium acetate by time-resolved small-angle X-ray scattering and rheology. *J. Phys. Chem. C*, **2015**,**119**:12660-12667

[22]Riello P, Minesso A, Craievich A, Benedetti A. Synchrotron SAXS study of the mechanisms of aggregation of sulfate zirconia sols. *J. Phys. Chem. B*, **2003**,**107**(15):3390-3399

[23]He J, Li H, Riisager A, Yang S. Catalytic transfer hydrogenation of furfural to furfuryl alcohol with recyclable Al-Zr@ Fe mixed oxides. *ChemCatChem*, **2018**,**10**(2):430-438

[24]Hu L, Li T, Xu J, He A, Tang X, Chu X, Xu J. Catalytic transfer hydrogenation of biomass-derived 5-hydroxymethylfurfural into 2,5-dihydroxymethylfuran over magnetic zirconium-based coordination polymer. *Chem. Eng. J.*, **2018**,**352**:110-119

[25]Zhang Y X, Wang X, Hou T, W, Huan L, Han L J, Xiao W H. Efficient microwave-assisted production of biofuel ethyl levulinate from corn stover in ethanol medium. *J. Energy Chem.*, **2018**,**27**(3):890-897

[26]He J, Xu Y F, Yu Z Z, Li H, Zhao W F, Wu H G, Yang S. $ZrOCl_2$ as a bifunctional and *in situ* precursor material for catalytic hydrogen transfer of bio-based carboxides. *Sustain. Energ. Fuels*, **2020**, **4**(5): 3102-3114

[27]Turan B, Sarigol G, Demircivi P. Adsorption of tetracycline antibiotics using metal and clay embedded cross-linked chitosan. *Mater. Chem. Phys.*, **2022**,**279**:125781

[28]Teufer G. The crystal structure of tetragonal ZrO_2. *Acta Crystallogr.*, **1962**,**15**(11):1187-1187

[29]Gossard A, Toquer G, Grandjean S, Grandjean A. Coupling between SAXS and Raman spectroscopy applied to the gelation of colloidal zirconium oxy-hydroxide systems. *J. Sol-Gel Sci. Technol.*, **2014**,**71**: 571-579

[30]Olliges-Stadler I, Rossell M D, Suess M J, Ludi B, Bunk O, Pedersen J S, Birkedal H, Niederberger M. A comprehensive study of the crystallization mechanism involved in the nonaqueous formation of tungstite. *Nanoscale*, **2013**,**5**:8517-8525

[31]Pedersen J S. Analysis of small-angle scattering data from colloids and polymer solutions: Modeling and least-squares fitting. *Adv. Colloid Interface Sci.*, **1997**,**70**:171-210

[32]Pedersen J S, Schurtenberger P. Scattering functions of semiflexible polymers with and without excluded volume effects. *Macromolecules*, **1996**,**29**:7602-7612

[33]Cates M E. Reptation of living polymers—Dynamics of entangled polymers in the presence of reversible chain-scission reactions. *Macromolecules*, **1987**,**20**(4):2289-2296

[34]Petitjean M. About the algebraic solutions of smallest enclosing cylinders problems. *Appl. Algebr. Eng. Commun. Comput.*, **2012**,**23**:151-164

[35]Singhal A, Keefer K D. A study of aluminum speciation in aluminum chloride solutions by small angle X-ray scattering and ^{27}Al NMR. *J. Mater. Res.*, **1994**,**8**:1973-1983